

SUPPORTING INFORMATION

Supplementary Information

for

Nanoemulsion fluorescent inks for anti-counterfeiting encryption with dual-mode, full-color and long-term stability

Wenna Wu,^a Huizhong Liu,^a Jin Yuan,^a Zhuo Zhang,^a Ling Wang,^a Shuli Dong,^a and Jingcheng Hao^{*a}

^a *Key Laboratory of Colloid and Interface Chemistry (Ministry of Education), Shandong University, Jinan 250100, China. E-mail: jaho@sdu.edu.cn, Fax: (+86) 531 88564464*

† Electronic Supplementary Information (ESI) available: Experimental details, synthesis, supplementary figures, tables, texts and references. See DOI: 10.1039/x0xx00000x

Table of Contents

- 1. Experimental procedures**
- 2. Results and discussions**
 - 2.1 Characterization of three-primary-color UC NPs and their upconversion luminescence properties**
 - 2.2 Downconversion fluorescence properties and mechanism**
 - 2.3 Preparation of O/W nanoemulsion**
 - 2.4 Phase transition**
- 3. Notes and references**

1. Experimental procedures

Chemical and materials. Rare-earth acetate salt $\text{Ln}(\text{CH}_3\text{CO}_2)_3 \cdot n\text{H}_2\text{O}$ ($\text{Ln} = \text{Gd}, \text{Er}, \text{Yb}, \text{Tm}, >99.9\%$), oleic acid (OA, tech. 90%) were purchased from Alfa Aesar Chemicals Co., Ltd. (China). 1-Octadecene (1-ODE, >90%), ammonium fluoride (NH_4F , >99.99%) were purchased from Aladdin Industrial Corporation (Shanghai, China). Sodium hydroxide (NaOH , >98%), sorbitan monooleate (Span 80), polyoxyethylene maleic anhydride monooleate (Tween 80), mineral oil were purchased from Sinopharm Chemical Reagent Co., Ltd. (China). Organic reagents such as hexane and ethanol were analytical grade and used without further purification. The water was obtained using a UPH-IV ultrapure water apparatus (China) with a resistivity of $18.25 \text{ M}\Omega \cdot \text{cm}$.

Characterizations. The cryo-TEM images of nanoemulsion were performed on a JEOL JEM-1400 TEM with a Gatan cryoplunge 3. High resolution transmission electron microscopy (HRTEM) images were obtained on a JEOL JEM-2100 TEM. Scanning electron microscopy (SEM) images were taken by a G300 FE-SEM System, Carl Zeiss. Fluorescence microscopy images were taken by an inverted fluorescence microscope Axio Observer 3. The luminescence spectra were recorded by using a Horiba FluoroMax-4 fluorescence spectrophotometer with an external 980 nm laser diode as the irradiation source. The luminescence lifetime decay profiles were conducted on Edinburgh Instruments Model FLS980 fluorescence spectrophotometer. The UV/Vis measurements were performed by a HITACHI U-4100 spectrophotometer (Hitachi, Japan). The size distribution of nanoemulsion droplets was measured on a Zetasizer Nano series (Malvern Instruments Ltd, UK). The dynamic viscosity of ink was measured using a Haake RheoStress 6000 Rheometer (Germany) with a Z_{41}Ti rotor drum and the surface tension was measured with a Processor Tensiometer K100 (KRUSS Company, Germany) by using plate method. The contact angle of ink was determined by commercial drop shape analyzer (Tracker, France Teclis). The printing images were performed by an HP Deskjet 1110 inkjet printer with a cartridge of 50 μm nozzle diameter. Multicolor images under NIR and UV irradiation are taken by using a Nikon D5200 camera with an infrared filter (>700 nm).

Synthesis of red-green-blue (RGB) upconversion nanoparticles (UC NPs). Synthesis of lanthanide-doped UC NPs was performed as previously reported by a thermal decomposition method with minor modifications.¹⁻⁵ In a typical synthesis process of green NaGdF_4 : 20% Yb^{3+} , 2% Er^{3+} , a mixture of 0.78 mmol $\text{Gd}(\text{CH}_3\text{CO}_2)_3 \cdot \text{H}_2\text{O}$, 0.2 mmol $\text{Yb}(\text{CH}_3\text{CO}_2)_3 \cdot 4\text{H}_2\text{O}$, 0.02 mmol $\text{Er}(\text{CH}_3\text{CO}_2)_3 \cdot 4\text{H}_2\text{O}$, 10 mL OA and 15 mL 1-ODE was firstly added into a 100 mL flask with stirring and then heated to 150 °C kept for 50 min under a nitrogen atmosphere. When the mixture cooled to room temperature, a methanol solution containing NaOH (2.5 mmol, 7 mL) and NH_4F (2.75 mmol, 3 mL) was quickly injected and heated to 50 °C kept for 30 min to proceed nucleation reaction. Then the mixture was heated to 110 °C for

SUPPORTING INFORMATION

2 h to get rid of methanol. Finally, the mixture was heated to 290 °C for 1.5 h with nitrogen protection. The resulting nanoparticles were precipitated by adding 2 mL ethanol, followed collected by centrifugation (8500 rpm, 5 min) and washed with hexane/ethanol (1:1 v/v) solution for three times, and then were dispersed in 4 mL of hexane.

To achieve coating NaGdF₄ shell on the NaGdF₄: Yb³⁺, Er³⁺ core, a mixture of 1 mmol Gd(CH₃CO₂)₃·H₂O, 10 mL OA, and 15 mL 1-ODE was heated to 150 °C for 50 min with nitrogen. Next, 4 mL NaGdF₄: Yb³⁺, Er³⁺ nanoparticles hexane solution and 10 mL methanol solution containing NaOH (2.5 mmol, 7 mL) and NH₄F (2.75 mmol, 3 mL) were injected in sequence. The subsequent steps were identical to synthesis of NaGdF₄:Yb³⁺, Er³⁺ core. Finally, the obtained core-shell NaGdF₄: Yb³⁺, Er³⁺@ NaGdF₄ nanoparticles were dispersed in 4 mL of hexane.

The synthesis of red NaGdF₄: 10% Er³⁺, 2% Tm³⁺ and blue NaGdF₄: 25% Yb³⁺, 0.3% Tm³⁺ was identical with green NaGdF₄: 20% Yb³⁺, 2% Er³⁺, except for the amounts and types of lanthanide dopants. For instance, 1.76 mmol Gd(CH₃CO₂)₃·H₂O, 0.2 mmol Er(CH₃CO₂)₃·4H₂O, and 0.04 mmol Tm(CH₃CO₂)₃·H₂O for red NaGdF₄: 10% Er³⁺, 2% Tm³⁺, 1.494 mmol Gd(CH₃CO₂)₃·H₂O, 0.5 mmol Yb(CH₃CO₂)₃·4H₂O, and 0.006 mmol Tm(CH₃CO₂)₃·H₂O for blue NaGdF₄: 25% Yb³⁺, 0.3% Tm³⁺.

Preparation of O/W nanoemulsion. O/W nanoemulsion was formed by diluting water-in-oil (W/O) microemulsion with water at elevated temperature.⁶⁻⁸ The surfactants (S) of Span 80 (HLB = 4.3, 53.27 wt%) and Tween 80 (HLB = 15, 46.73 wt%) were mixed to form mixed emulsifier (HLB = 10), which was dissolved into mineral oil (O) under magnetic stirring. Then the water was added into oil-surfactants mixtures with different weight ratio from O:S = 9:1 to 1:9 until it became turbid by clarification to prepare W/O microemulsion. Next, the ternary phase diagram of the water/Span 80-Tween 80/oil systems was taken to select region of W/O microemulsion (Fig. S7). Taking droplets size and viscosity of emulsion into consideration, we chose O:S = 1:1 and 4:1 as research objects. Eventually, the microemulsion and water were placed separately in a water bath at 70 °C. The large amount of water (2 g and 3 g) was quickly and respectively added into both of W/O microemulsion with O:S = 1:1 and 4:1, where surfactant molecules occurred migrate and reverse to form new oil-water interfaces leading to the spontaneous formation of O/W nano-droplets. After the dilution, the samples were cooled at room temperature and four types of O/W nanoemulsion were successfully prepared, respectively named as N₁ (C_{oil} = C_{surfactant} = 16.7 wt%, C_{water} = 66.7 wt%), N₂ (C_{oil} = C_{surfactant} = 12.5 wt%, C_{water} = 75 wt%), N₃ (C_{oil} = 26.6 wt%, C_{surfactant} = 6.7 wt%, C_{water} = 66.7 wt%), and N₄ (C_{oil} = 20 wt%, C_{surfactant} = 5 wt%, C_{water} = 75 wt%).

Preparation of RGB luminescent anti-counterfeiting inks. Water-based inks were prepared based on above four O/W nanoemulsions, in which luminescent nanoparticles can be encapsulated into oil droplets and form nanoemulsion inks. The synthetic method of nanoparticles-encapsulated nanoemulsions was identical to the blank

SUPPORTING INFORMATION

nanoemulsions, except that hexane solution containing luminescent UC NPs and CQDs was added into microemulsion at 70 °C before dilution where hydrophobic UC NPs and CQDs can uniformly disperse in oil phase of microemulsion. The mixtures were continuously heated for 20 min at 70 °C to evaporate hexane solvent. Then water was added to dilute microemulsion forming O/W nanoemulsion where hydrophobic UC NPs and CQDs can be uniformly encapsulated inside oil droplets. After the samples were cooled at room temperature, the four types of luminescent water-based anti-counterfeiting inks were successfully prepared. Inks with RGB or different fluorescence colors were prepared by adjusting the ratio of red, green and blue fluorescent nanoparticles.

Physical and chemical properties measurements of inks. (1) To determine the dynamic viscosity of four type water-based anti-counterfeiting inks, rheological tests of steady shear were performed. 12 mL emulsion was loaded into a rotor drum to measure at room temperature with frequency sweeping from 0.001 to 1000 s⁻¹. (2) The surface tension of emulsion inks was determined by using surface tension meter with a plate method, where each type emulsion was selected as mother solution. Each value is the average of three measurements. (3) The density of inks was measured by mass volume method. According to the definition of $\rho = m/v$, we measured mass and volume of inks and then could calculate the density of inks. Each value was measured three times. (4) The contact angle on different substrates was measured to evaluate the hydrophilicity of inks. Paper substrates (including commercial A4 paper, experimental filter paper and weigh paper) and glass slide substrates were selected as research objects.

Testing the long-term stability of nanoemulsions inks. Long-term stability of the nanoemulsions inks with different ratios of O/S/W was determined by observing the macroscopic appearance and measuring droplet size at different intervals over a six-month period. The sample was diluted about 500 times with deionized water just before the measurements of droplet size via dynamic light scattering. Measurements were carried out 3 times for each nanoemulsion, and then the average droplet size and the corresponding standard deviation were obtained. During studies, the nanoemulsion inks were enclosed in a small glass bottle without shake at 25 °C.

Application and dual-mode imaging of inkjet printing, stamping and writing. RGB three types of inks were injected into an empty print cartridge with 50 μm nozzle diameters which were installed into the HP Deskjet 1110 inkjet printer and tested separately for printing on the paper substrate and PVC thin films. An ink pen was loaded with inks for writing on the paper substrate. The stamper was dipped into inks for stamping on the paper substrate. All the luminescent patterns on paper or PVC thin films were invisible in sunlight but visible in darkroom under the 980 nm CW laser irradiation (20 W/cm² power density) and 365 nm UV lamp. The images of the patterns were obtained using a Nikon D5200 camera with an infrared filter. The exposure time was 20 s, aperture size used was F4.0.

SUPPORTING INFORMATION

2. Results and discussion

2.1 Characterization of three-primary-color UC NPs and their upconversion luminescence properties.

Green core NaGdF₄: 20% Yb³⁺, 2% Er³⁺ UC NPs was firstly synthesized by using a thermal decomposition method with modified. Fig. S1a is the TEM image of UC NPs with an average diameter of about 6.26 nm (Fig. S2a). The upconversion fluorescence emission spectrum of core OA-UC NPs by 980 nm laser irradiation was recorded in Fig. S1b, presenting weak fluorescence intensity due to large surface defects. In order to enhance fluorescence intensity, core OA-UCNPs are served as seed crystal to regrow shell NaGdF₄ on the surface of NaGdF₄: Yb³⁺, Er³⁺. Fig. S(1c and 3a) are TEM and SEM images of core-shell NaGdF₄: Yb³⁺, Er³⁺@NaGdF₄ UCNPs, respectively. The average diameter increases to approximately 15.0 nm (Fig. S2b). Compared with Fig. S1b, the UC fluorescence intensity of NaGdF₄: Yb³⁺, Er³⁺@NaGdF₄ (Fig. S1d) is significantly enhanced after epitaxial shell layer growth, this is because thin-shell coating largely reduces surface defect density and preserves the optical integrity of the nanoparticles. The major four emission peaks can be observed at 407, 520, 540, and 654 nm in Fig. S1d, corresponding to the transitions of ²H_{9/2}→⁴I_{15/2}, ²H_{11/2}→⁴I_{15/2}, ⁴S_{3/2}→⁴I_{15/2}, and ⁴F_{9/2}→⁴I_{15/2} of Er³⁺ respectively,⁹ which is identical to Fig. S1b.

To prepare blue color and red color luminescent UC NPs and avoid the defect of fluorescence quenching caused by small size nanoparticles, we altered doped ions and increased doping amounts of 25% Yb³⁺, 0.3% Tm³⁺ and 10% Er³⁺, 2% Tm³⁺ into NaGdF₄ matrix, respectively. The two samples were denoted as UC NPs-B and UC NPs-R. Fig. S(1e and 3b) are the TEM and SEM images of UC NPs-B NaGdF₄: Yb³⁺, Tm³⁺, respectively, with uniform and large-size hexagonal shapes, showing that excellent blue fluorescence emission due to the intensity of blue emission peaks at 479 nm was significantly higher than that of the red peak at 654 nm, corresponding to ¹D₂→³F₄, ¹G₄→³H₆ and ¹G₄→³F₄ transitions of Tm³⁺ with 980 nm laser excitation, respectively (Fig. S1f).⁹ Fig. S(1g and 3c) are the TEM and SEM images of UC NPs-R NaGdF₄: Er³⁺, Tm³⁺, and Fig. S1h is the fluorescence emission spectrum of UC NPs-R, and the main peak position is located at 654 nm due to ⁴F_{9/2}→⁴I_{15/2} transition of Er³⁺ by 980 nm NIR excitation.⁹ As shown in Fig. S1i, the three-primary-color upconversion fluorescence of the RGB UC NPs was labeled in the CIE color coordinates. It can be seen that the three positions of the RGB UC NPs could make up a triangle covering almost half of the region of the chromaticity diagram. It means that full-colors including white could be obtained based on mixing the RGB UC NPs in a proper ratio. Overall, the OA-stabilized RGB UC NPs with high stability, strong upconversion fluorescence intensity and tunable fluorescence emission color could be a suitable fluorescence tag in anti-counterfeiting inks applications.

SUPPORTING INFORMATION

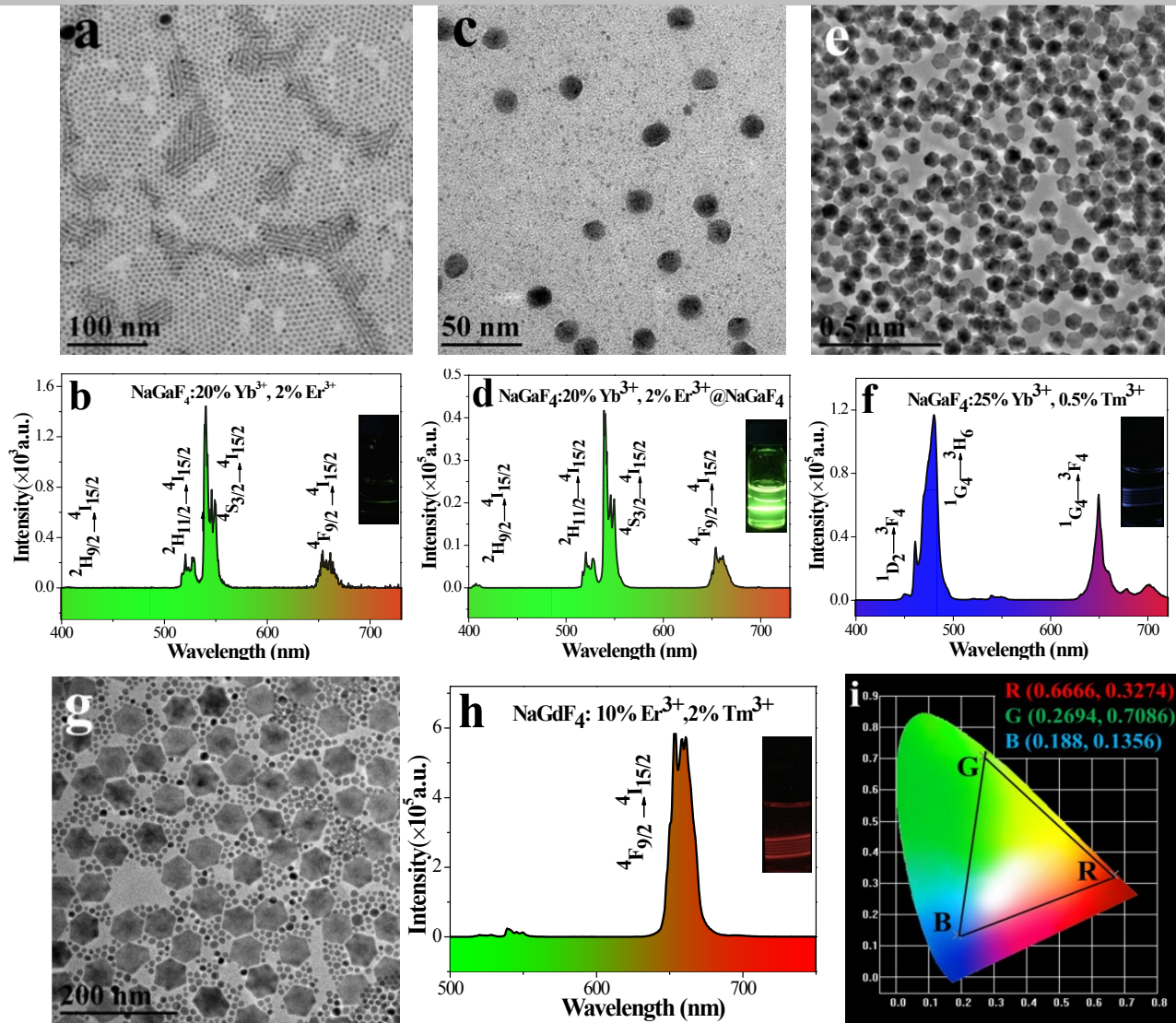
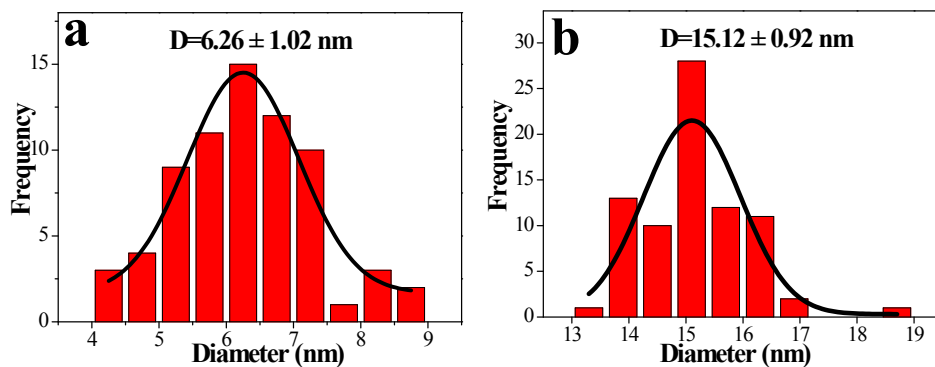


Fig. S1. TEM images (a) and upconversion emission spectra (b) of green NaGdF₄: Yb³⁺, Er³⁺; (c and d) green NaGdF₄: Yb³⁺, Er³⁺@NaGdF₄; (e and f) blue NaGdF₄:Yb³⁺, Tm³⁺; (g and h) red NaGdF₄: Er³⁺, Tm³⁺ UC NPs, respectively. (Insets are the images of UC NPs dispersed in hexane with 980 nm laser). (i) The positions of the upconversion emission of RGB UC NPs within the CIE color coordinates, where the UC NPs-R, UC NPs-G, and UC NPs-B were (0.6666, 0.3274), (0.2694, 0.7086) and (0.188, 0.1356), respectively.



SUPPORTING INFORMATION

Fig. S2. Particle size statistics of core NaGdF₄: Yb³⁺, Er³⁺ and core-shell NaGdF₄: Yb³⁺, Er³⁺@NaGdF₄ UC NPs.

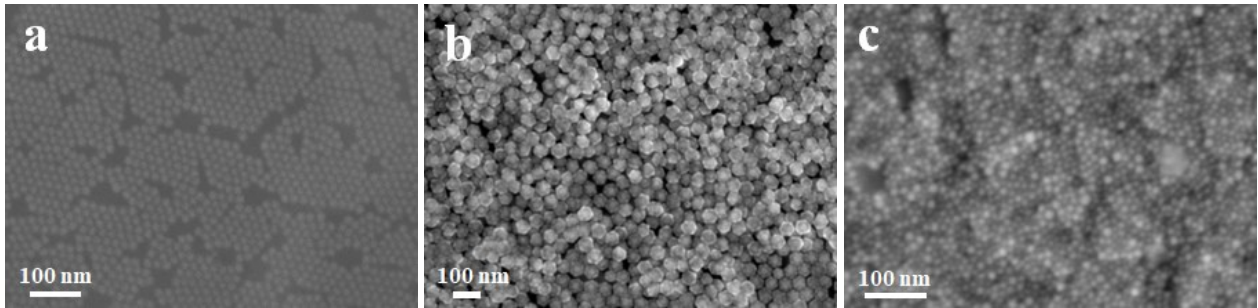


Fig. S3. SEM images of (a) core-shell NaGdF₄: Yb³⁺, Er³⁺@NaGdF₄ UC NPs-G, (b) NaGdF₄:Yb³⁺, Tm³⁺ UC NPs-B, and (c) NaGdF₄: Er³⁺, Tm³⁺, UC NPs-R.

2.2 Downconversion fluorescence properties and mechanism

Firstly, the NPs with normal condition was synthesized under nitrogen protection, which prevented oleic acid molecules from oxidization by the air. Therefore, the generated pure surface state on the surface of CQDs caused wide energy level distribution,¹⁰ which can capture a wide range of excitation energy and presented excitation-dependent fluorescence phenomenon in Fig. S4b. However, the NPs with changed condition was synthesized with the participation of oxygen caused oleic acid oxidizing, which will introduce a new surface state onto the surface of CQDs undermining and passivating the original surface state. This new surface state leading to a single defect site might capture a narrow range of excitation energy and generate excitation-independent fluorescence property in Fig. 1f. In addition, excitation-dependent fluorescence characteristics may be relevant to size distribute.¹¹ From Fig. S5e we can see CQDs in NPs with normal condition presented wide size distribution which meant the existence of multiple energy gaps resulting in various transition patterns. When there were different excitation wavelengths, different transition modes would dominate and consequently showed excitation-dependent fluorescence characteristics in Fig. S4b. On the contrary, the CQDs of NPs with changed condition in Fig. S5c had a relatively narrow size distribution resulting single energy gaps. Different excitation wavelengths showed the same transition, and the emission wavelength will not change with the increase of excitation wavelength, therefore CQDs presented independent fluorescence characteristics of excitation in Fig. 1f.

SUPPORTING INFORMATION

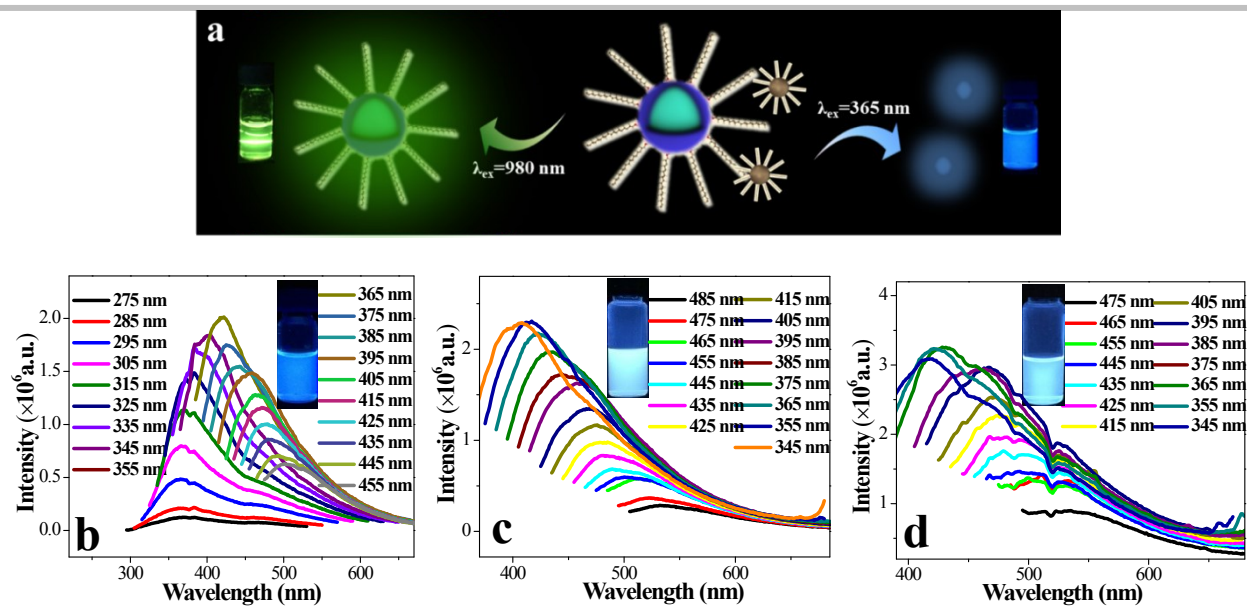


Fig. S4. (a) Schematic illustration of dual-mode fluorescent under 980 nm irradiation and 365 nm UV light. (b) (c) (d) are DC fluorescence emission spectra of UC NPs-G, UC NPs-B and UC NPs-R, respectively. (Insets are the images of UC NPs dispersed in hexane with 365 nm lamp excitation).

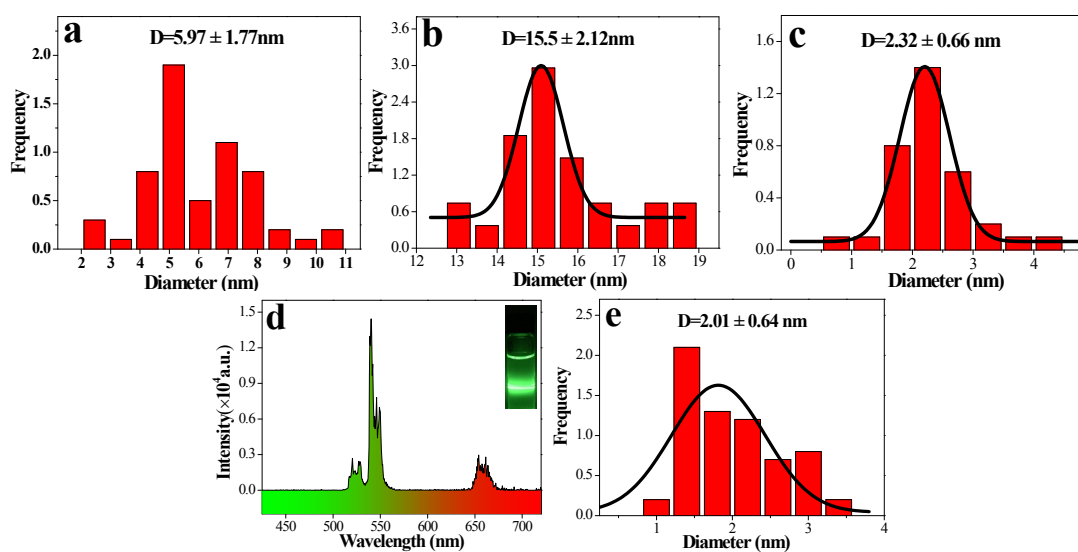


Fig. S5. (a) The size distribution of CQDs in blank control experiment. The size statistics of UC NPs (b) and CQDs (c), and upconversion fluorescence emission spectrum (d) of products under changing synthetic conditions. (e) The size distribution of CQDs in normal experiment.

SUPPORTING INFORMATION

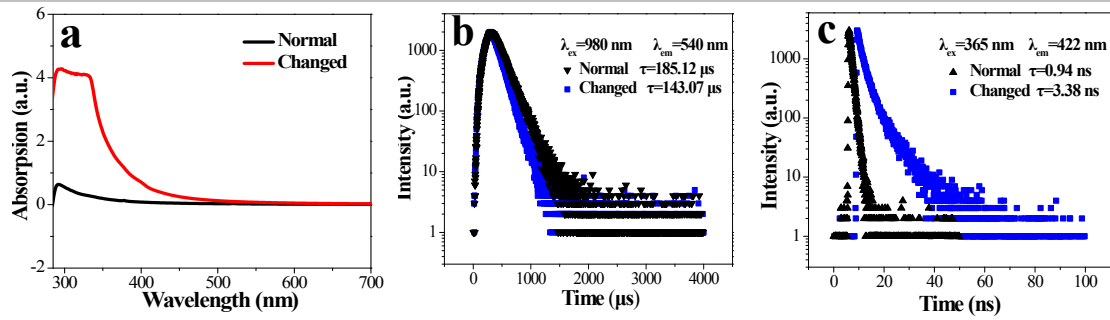


Fig. S6. (a) Ultraviolet absorption profiles of NPs with normal condition and changed condition, respectively. (b) Upconversion luminescence lifetime decay profiles. (c) Downconversion luminescence lifetime decay profiles.

2.3 Preparation of O/W Nanoemulsion

Water-based anti-counterfeiting inks can be acquired by encapsulating dual-mode luminescent nanoparticles into oil droplets of an O/W NE (Fig. S7). The emulsion system must meet some requirements to be selected as a water-based inks for inkjet printing. The first one is that the droplet size of the O/W emulsion should be larger than those of encapsulated UC NPs and QCDs. The nanoparticles may be stably carried into the oil droplets. The second one is that the emulsion should have a high boiling point and low viscosity to keep the nozzle moist and prevent nozzle blocking. Before the preparation of NPs-encapsulated emulsions, the hydrophobic properties and stability of CQDs must be first confirmed *via* a phase transition method, and the results are shown in Fig. S8, suggesting that the QCDs are hydrophobic and the ligands are stably combined with the surface, leading to the excellent dispersion in oil solvent. One of the key factors for the formation of stable emulsion inks is the surfactant hydrophilic-lipophilic balance (HLB) value.¹² In this study, we selected Span 80 (HLB = 4.3) and Tween 80 (HLB = 15) as mixed emulsifiers (HLB = 10) whose HLB value differ greatly in order to greatly enhance the emulsification effect. The water/Span 80-Tween 80/oil microemulsion systems are selected to prepare O/W NEs. As shown in Fig. S7, the ternary phase diagram was obtained to select the W/O microemulsion region. To meet the above two requirements, two W/O microemulsions in the selected region of phase diagram with oil (O) to surfactant (S) weight ratio of 1:1 and 4:1 were chosen to dilute. The temperature and water amount may largely affect the size of oil droplets, because the increasing temperature and water amount would reduce viscosity of oil phase and improve the migration rate of surfactants.¹³ In this study the emulsion preparation temperature was fixed at 70°C and different amounts of water (2 and 3 g) were, respectively, added into the two W/O microemulsions to form four milk-white NEs, named as N_1 ($C_o = C_s = 16.7\text{ wt}\%$, $C_w = 66.7\text{ wt}\%$), N_2 ($C_o = C_s = 12.5\text{ wt}\%$, $C_w = 75\text{ wt}\%$), N_3 ($C_o = 26.6\text{ wt}\%$, $C_s = 6.7\text{ wt}\%$, $C_w = 66.7\text{ wt}\%$), and N_4 ($C_o = 20\text{ wt}\%$, $C_s = 5\text{ wt}\%$, $C_w = 75\text{ wt}\%$), respectively.

SUPPORTING INFORMATION

The four types of nanoemulsions were, respectively, stained with oil-soluble perylene red dye and then characterized using the fluorescence microscopy images in Fig. S9(a-d), where one can see that the oil droplets are uniformly dispersed in the continuous water phase, indicating that the type of emulsion is an O/W NE. A further investigation of the morphologies of the NEs by cryo-TEM (Fig. 2(a-d)) reveals that there are not only spherical NE droplets but also some vesicles coexisting with them. A similar phenomenon has been reported by McCormick *et al.*,^{14,15} which may be attributed to the type of diluted microemulsion and the mass fraction of water. For samples of NE N₁ in Fig. 2a, emulsion droplets and vesicles coexist. With the increase of water mass fraction, a system dominated by emulsion droplets forms, as shown in Fig. 2b. This may be ascribed to the formation of a layered mesophase that can easily flake into vesicles and form monodispersed NEs with small particle size. The same principle is suitable for explaining the phenomenon in Fig. 2(c and d). In addition, the droplets size of the NEs is determined by dynamic laser light scattering (DLS) after letting them sit for one day as shown in Fig. S10. It can be seen that the size of the droplets gradually increases with the increasing ratio of oil to surfactant or the increasing amount of water, which is consistent with the results of the fluorescence microscopy images in Fig. S9(a-d). This may be because the decrease of the surfactant concentration used to stabilize the NE leads to an increase in the interface energy of the oil-water interface. The hydrodynamic diameter of the NE determined by DLS is sufficiently larger than the size of the fluorescent nanoparticles, which is thus beneficial for nanoparticles to be perfectly encapsulated inside the oil droplets.

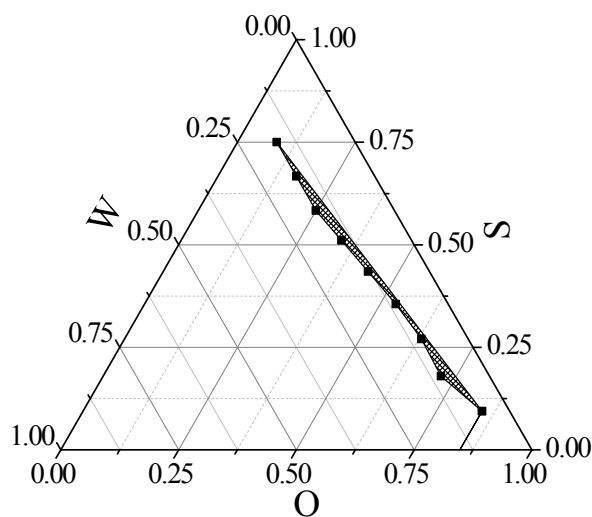


Fig. S7. The ternary phase diagram of water/Span 80-Tween 80/oil systems, the selected region is W/O microemulsion.

2.4 Phase transition

The NPs with normal condition (1) and changed condition (2) both emitted strong blue downconversion luminescence and green upconversion luminescence in hexane under 980 nm laser and 365 nm lamp excitation,

SUPPORTING INFORMATION

respectively (Fig. S8a). Phase transfer was conducted by mixing acid alcohol solution and NPs in hexane (Fig. S8b). Then the mixture was suffered from vigorous stir and ultrasound to achieve phase transfer. Subsequently, the top layer of hexane and bottom layer of water were separated. It can be seen in Fig. S8c that both UC NPs of NPs-1 and NPs-2 successfully transferred from the top hexane layer to the bottom water layer due to the surface hydrophobic ligands protonation and then removal from the surface of UC NPs, while the QCDs were still in the oil phase. The fluorescence emission spectrum may further illustrate that the UC NPs transferred into water but QCDs had no transformation in Fig. S8d and Fig. S8e. All these results confirmed that the QCDs were hydrophobic and the ligands may covalently combine to the surface, which can be highly stable and well dispersed in oil solve. Therefore, we can favorably encapsulate hydrophobic UC NPs and QCDs into oil droplets of O/W emulsion to prepare dual-mode luminescent anti-counterfeiting inks.

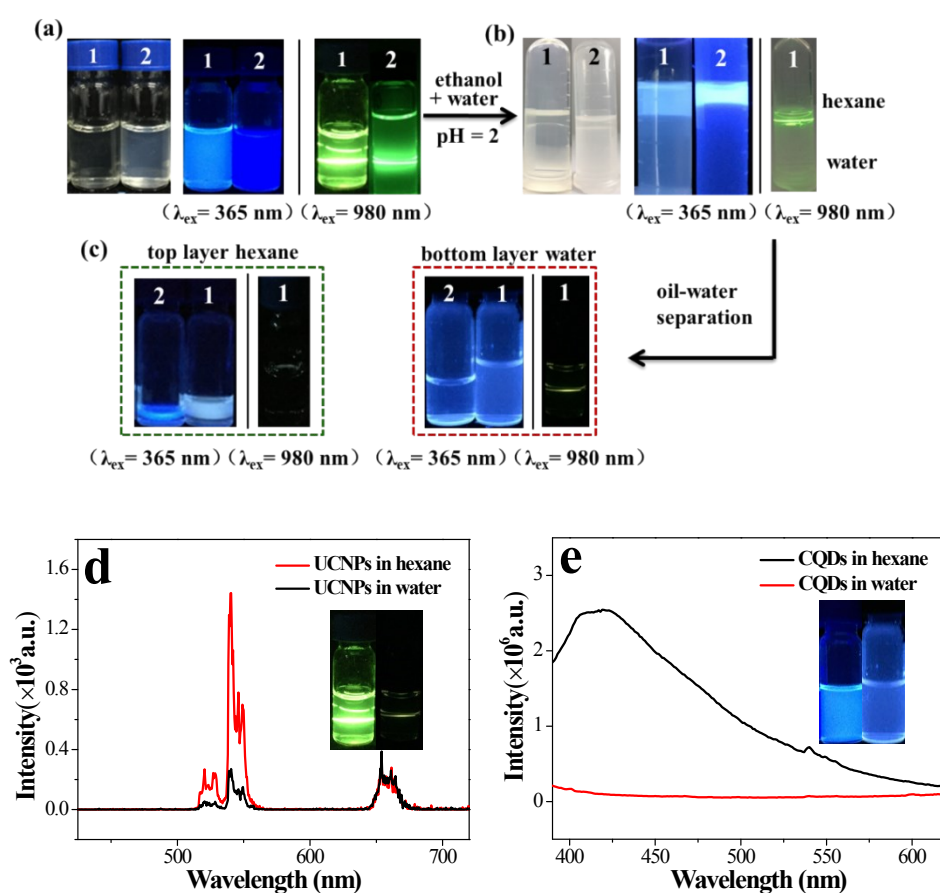


Fig. S8. (a) (b) (c) Schematics of NPs with normal condition (1) and changed condition (2) phase transformation. (d) The upconversion fluorescence emission spectrum of UC NPs and (e) downconversion fluorescence emission spectrum of QCDs before and after phase transformation.

SUPPORTING INFORMATION

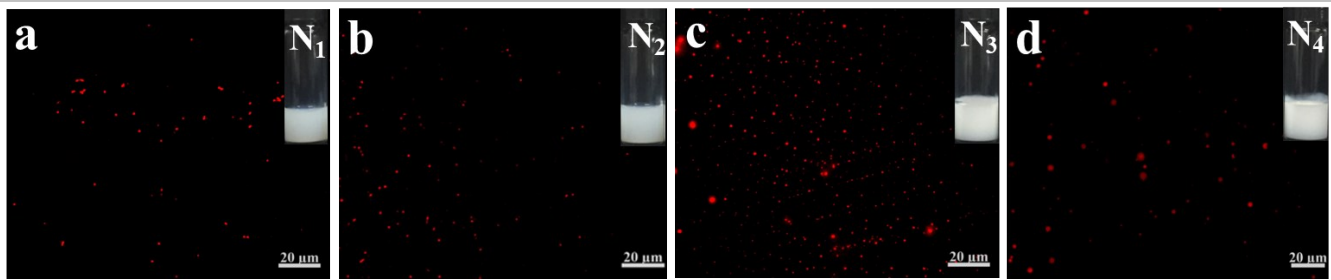


Fig. S9. (a-d) Fluorescence microscope images of four types O/W nanoemulsion, respectively N_1 ($C_{oil} = C_{surfactant} = 16.7$ wt%, $C_{water} = 66.7$ wt%), N_2 ($C_{oil} = C_{surfactant} = 12.5$ wt%, $C_{water} = 75$ wt%), N_3 ($C_{oil} = 26.6$ wt%, $C_{surfactant} = 6.7$ wt%, $C_{water} = 66.7$ wt%), and N_4 ($C_{oil} = 20$ wt%, $C_{surfactant} = 5$ wt%, $C_{water} = 75$ wt%).

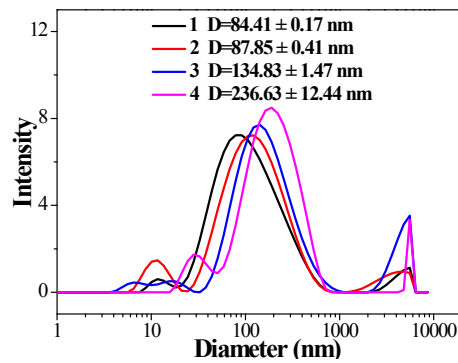


Fig. S10. The droplets size of the nanoemulsions inks by DLS after standing one day.

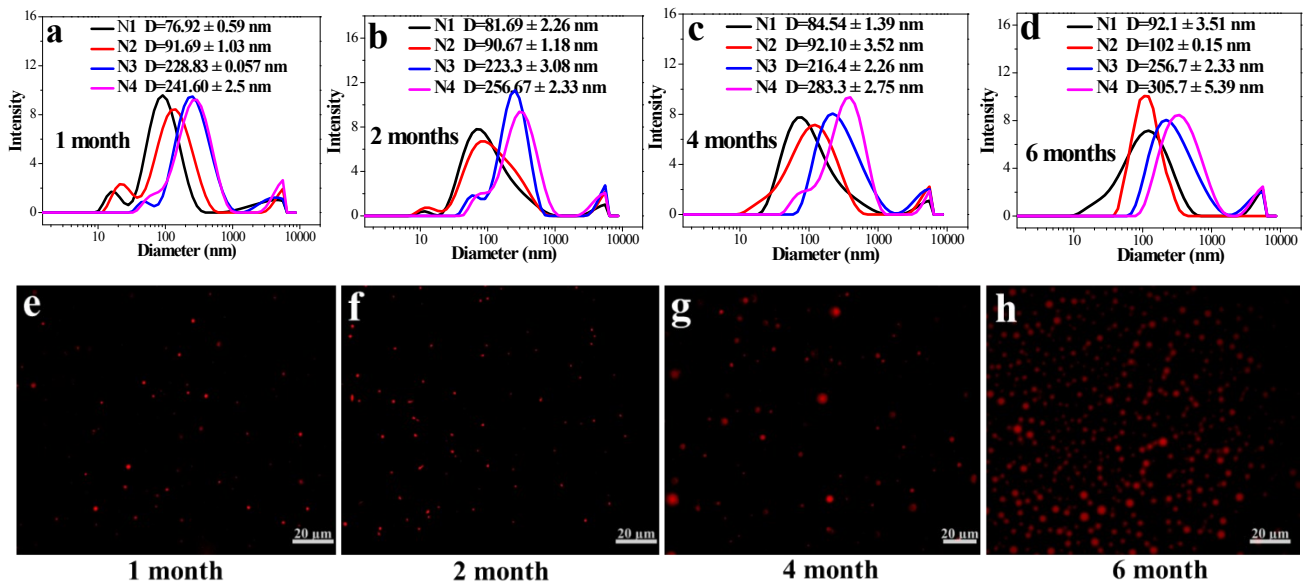


Fig. S11. (a-d) The size characterizations of four nanoemulsion inks by DLS in different period (respectively 1, 2, 4, 6 months). (e-h) The fluorescence microscope images of N_2 nanoemulsion inks in different period (respectively 1, 2, 4, 6 months).

SUPPORTING INFORMATION

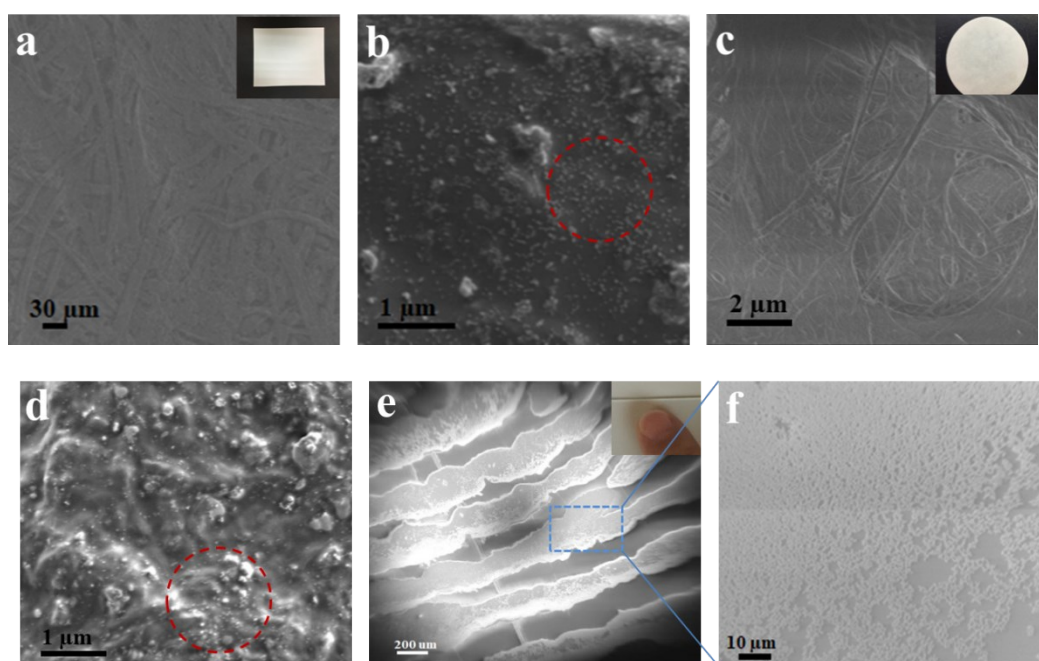


Fig. S12. SEM images of (a) bare A4 paper and (c) bare filter paper compared to inks dipped on (b) A4 paper and (d) filter paper, respectively. (e) SEM images of fingerprints patterns and (f) the magnifying SEM images.

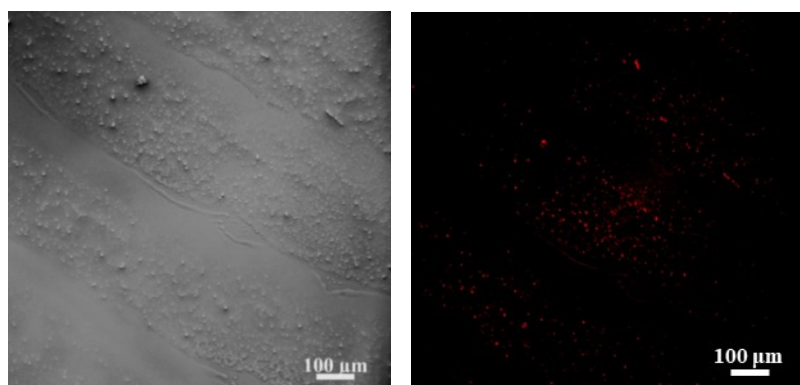


Fig. S13. Daylight microscope image (left) and fluorescence microscope image (right) of fingerprint pattern dipped with inks on glass slide.

SUPPORTING INFORMATION

Table S1. Contact Angles (CAs) of NE inks droplets on different substrate.

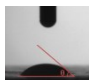
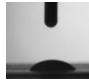
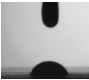
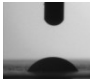
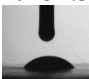

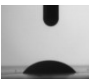


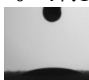
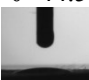
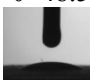
Substrate	N ₁	N ₂	N ₃	N ₄
A4 paper	 $\theta=32.3^\circ$	 $\theta=43.0^\circ$	 $\theta=60.6^\circ$	 $\theta=50.4^\circ$
Weight paper	 $\theta=33.4^\circ$	 $\theta=47.1^\circ$	 $\theta=44.5^\circ$	 $\theta=48.5^\circ$
Filter paper	 $\theta=26.0^\circ$	 $\theta=8.3^\circ$	 $\theta=14.8^\circ$	 $\theta=26.9^\circ$

Table S2. Physical and chemical parameters of nanoemulsions inks.

Parameter	N ₁	N ₂	N ₃	N ₄
γ (mN·m ⁻¹)	31.10	30.35	31.20	30.43
ρ (g·cm ⁻³)	0.98	0.98	0.938	0.97
η (mPa·s)	19.88	8.61	6.81	4.28
α (μm)	50	50	50	50
Z	1.96	4.48	5.60	8.95

SUPPORTING INFORMATION

3. Notes and references

- 1 W. Wu, L. Wang, J. Yuan, Z. Zhang, X. Zhang, S. Dong, J. Hao, *Macromolecules* 2020, **53**, 2430-2440.
- 2 F. Wang, R. Deng, X. Liu, *Nat. Protoc.* 2014, **9**, 1634-1644.
- 3 W. Wu, L. Wang, Y. Wang, L. Guo, S. Dong, J. Hao, *J. Colloid Interf. Sci.* 2020, **563**, 308-317.
- 4 M. L. You, M. Lin, S. R. Wang, X. M. Wang, G. Zhang, Y. Hong, Y. Q. Dong, G. R. Jin, Feng Xu, *Nanoscale* 2016, **8**, 10096-10104.
- 5 J. M. Meruga, A. Baride, W. Cross, J. J. Kellara, P. S. May, *J. Mater. Chem. C* 2014, **2**, 2221-2227.
- 6 I. Solè, C. Solans, A. Maestro, C. González, J. M. Gutiérrez, *J. Colloid Interf. Sci.* 2012, **376**, 133-139.
- 7 L. J. Yu, C. Li, J. Xu, J. C. Hao, D. J. Sun, *Langmuir* 2012, **28**, 14547-14552.
- 8 K. Tong, C. H. Zhao, D. J. Sun, *Colloids Surfaces A* 2016, **497**, 101-108.
- 9 S. Xie, C. Tong, H. Tan, N. Li, L. Gong, J. Xu, L. Xu, C. Zhang, *Mater. Chem. Front.* 2018, **2**, 1997-2005.
- 10 J. Wang, C. M. Cheng, Y. Huang, B. Z. Zheng, H. Y. Yuan, L. Bo, M. W. Zheng, S. Y. Yang, Y. Guo, D. Xiao, *J. Mater. Chem. C* 2014, **2**, 5028-5035.
- 11 X. M. Li, Y. L. Liu, X. F. Song, H. Wang, H. S. Gu, H. B. Zeng, *Angew Chem. Int. Ed.* 2015, **54**, 1759-1764.
- 12 L. Wang, K. J. Mutch, J. Eastoe, R. K. Heenan, J. Dong, *Langmuir* 2008, **24**, 6092-6099.
- 13 L. Yu, C. Li, J. Xu, J. Hao, D. Sun, *Langmuir* 2012, **28**, 14547-14552.
- 14 H. S. Lee, E. D. Morrison, C. D. Frethem, J. A. Zasadzinski, A. V. McCormick, *Langmuir* 2014, **30**, 10826-10833.
- 15 P. M. de Molina, M. Zhang, A. V. Bayles, M. E. Helgeson, *Nano Lett.* 2016, **16**, 7325-7332.